NANO LETTERS

pubs.acs.org/NanoLett

Letter

Atomically Smooth Single-Crystalline Platform for Low-Loss Plasmonic Nanocavities

Lufang Liu,[‖] Alexey V. Krasavin,[‖] Junsheng Zheng, Yuanbiao Tong, Pan Wang,* Xiaofei Wu, Bert Hecht, Chenxinyu Pan, Jialin Li, Linjun Li, Xin Guo, Anatoly V. Zayats,* and Limin Tong*

Cite This: *Nano Lett.* 2022, 22, 1786−1794

Read Online

ACCESS | Metrics & More | Article Recommendations | Supporting Information

ABSTRACT: Nanoparticle-on-mirror plasmonic nanocavities, capable of extreme optical confinement and enhancement, have triggered state-of-the-art progress in nanophotonics and development of applications in enhanced spectroscopies. However, the optical quality factor and thus performance of these nanoconstructs are undermined by the granular polycrystalline metal films (especially when they are optically thin) used as a mirror. Here, we report an atomically smooth single-crystalline platform for low-loss nanocavities using chemically synthesized gold microflakes as a mirror. Nanocavities constructed using gold nanorods on such microflakes exhibit a rich structure of plasmonic modes, which are highly sensitive to the thickness of optically thin (down to ∼15 nm) microflakes. The microflakes endow nanocavities with significantly improved quality factor (∼2 times) and scattering intensity (∼3 times) compared with their counterparts based on deposited films. The developed low-loss nanocavities further allow for the integration with a mature platform of fiber optics, opening opportunities for realizing nanocavity-based miniaturized photonic devices for practical applications.

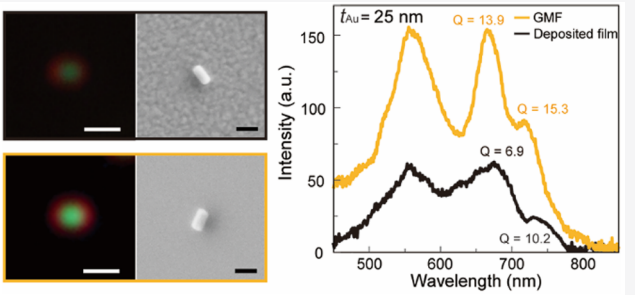

KEYWORDS: *Plasmonics, nanocavity, single-crystalline, gold microflakes, nanorod*

The ability to truly confine and modulate light on the nanoscale allows access to the regime of extreme light−matter interactions for fundamental studies as well as the realization of highly compact nanophotonic devices. By coupling optical fields with collective electronic excitations (i.e., surface plasmons), plasmonic nanoparticles have the ability to confine light down to a deep-subwavelength scale (e.g., 10 nm) and produce enhanced local electromagnetic fields.[1,2] However, it is challenging to achieve more tightly confined optical fields (e.g., sub-5 nm).[3] Recently, nanoparticle-on-mirror (NPoM) plasmonic nanocavities,[4,5] formed by placing a metal nanoparticle on a metal film separated with a nanometer-thick dielectric layer, have attracted intensive research interest due to their capability of extreme optical confinement and ease of fabrication.[6−9] They have given rise to a series of breakthroughs in state-of-the-art nanophotonic research and applications,[10−29] such as spontaneous emission enhancement,[13,15,17] strong coupling,[16,18,25] optical sensing,[11,19,27,28] and quantum plasmonics.[20,21] Usually, the implementation of NPoM nanocavities uses deposited metal films as the mirror,[6−9,11−19,21−29] which have a polycrystalline structure and a typical surface root-mean-square (RMS) roughness of a few nanometers.[4] Due to the extreme confinement of the optical fields in the nanometer-scale gap, granular polycrystalline metal films can introduce a significant optical loss because of the scattering of electrons by surface roughness and numerous grain boundaries.[30−35] This limits the optical quality of NPoM nanocavities and prevents achieving and exploiting multiresonant nanocavities as closely spaced resonances become merged due to the low quality factors, which inevitably degrade the performance of the nanocavities. The poor surface quality can further cause a deviation of the optical response of an NPoM nanocavity from the designed parameters and significant cavity-to-cavity variation of the optical response due to the fluctuation in the gap geometry and thickness.[36] Therefore, improving the structural quality of metal mirrors is critical to exploit the full potential of NPoM nanocavities. By use of template-stripped metal films,[37] the RMS roughness of the metal surface in contact with an ultrasmooth substrate can be as low as ∼0.2 nm,[38] which is beneficial for the improvement of the optical quality of NPoM nanocavities.[4,15,22] Thermal annealing of the metal films before stripping can further increase the grain sizes to reduce the loss due to scattering of electrons at grain boundaries.[31] However, as-prepared metal films retain the polycrystalline structure, and

Received: January 10, 2022
Revised: January 27, 2022
Published: February 7, 2022

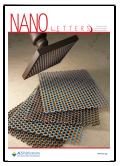

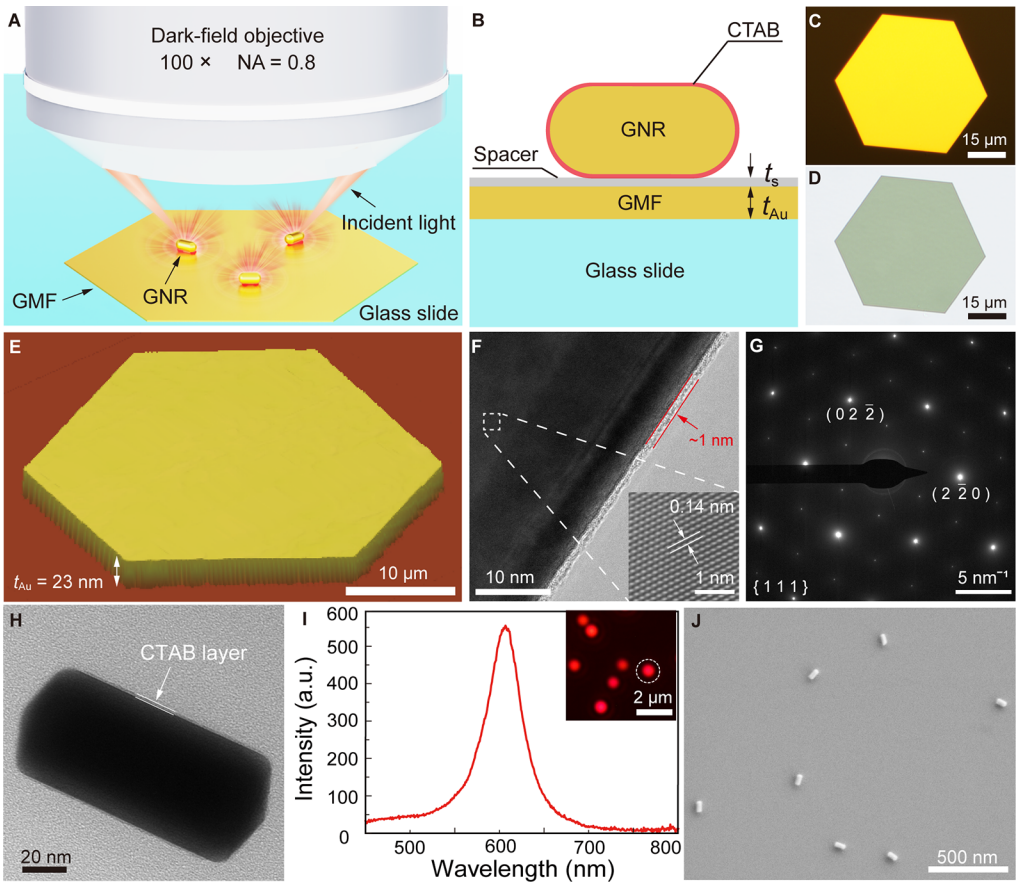

Figure 1. Design of NRoMF nanocavities. (A) Schematic representation and (B) a cross-sectional view of a GNR on a GMF separated by a dielectric spacer. Illumination condition in a dark-field microscope is also shown in (A). (C, D) Optical micrographs of a GMF (t_{Au} = 27 nm) taken in (C) reflection and (D) transmission. (E) AFM image of a GMF. (F) TEM image of an edge of a GMF showing the existence of a native organic layer. Inset: high-resolution TEM image of the GMF. (G) Corresponding electron diffraction pattern of the GMF. (H) TEM image of a GNR. (I) Scattering spectrum of a GNR on a glass slide under unpolarized excitation and detection. Inset: dark-field scattering image of the measured GNR (circled). (J) Scanning electron microscopy (SEM) image of NRoMF nanocavities formed on a GMF.

the rough surface at the opposite side of the film still has an obvious effect on the optical quality of nanocavities constructed on optically thin metal films, especially when the access through the film is needed, as in the case of nanocavities integrated with other optical devices or systems (e.g., optical waveguides). In addition, with this approach it is challenging to fabricate an integrated metallic mirror in a targeted device. Therefore, to date, NPoM nanocavities are mostly formed on nontransparent thick metal mirrors. At the same time, their excitation is usually conducted from the nanoparticle side using bulky optical microscopy systems,[4] making it difficult to compactly integrate nanocavities with other optical devices or systems (where the excitation from the substrate side is required) for practical applications. It is still a challenge to realize low-loss NPoM nanocavities especially when the metal mirrors are optically thin, which are attractive for further engineering nanocavity modes via decreasing of the mirror thickness and accessing the nanocavity modes from the substrate side.

Here, by using atomically smooth single-crystalline gold microflakes (GMFs) with tunable thickness down to ~15 nm as a mirror, we report a new platform for NPoM nanocavities with superior optical properties in terms of GMF thickness-dependent mode structure tunability together with significantly improved quality factor (~2 times) and scattering intensity (~3 times) compared with their counterparts based on deposited films. The use of plasmonic nanorods to define a cavity further provides a multiresonant response, in contrast to nanospheres, which is important for nonlinear optics and sensing applications. Moreover, the transferable GMFs allow for the facile integration of low-loss nanocavities with mature platform of fiber optics, where optically thin ultrasmooth mirrors allow excitation through the substrate, opening new opportunities for developing nanocavity-based photonic devices with miniaturized sizes.

RESULTS AND DISCUSSION

Fabrication of Nanocavities. In order to achieve multiresonant high-Q nanocavities capable of operating in a broad spectral range,[39] gold nanorods (GNRs) were used to define cavities on GMFs, i.e., nanorod-on-microflake (NRoMF) nanocavities (Figure 1A,B). Single-crystalline GMFs, with thicknesses tunable in the range of ~10−300 nm, were chemically grown on a glass slide[40,41] (Supporting Information Section 1). Figure 1C shows an optical micrograph of a GMF with a thickness of 27 nm, which is semitransparent and gives a greenish color in transmission due to the relatively small thickness (Figure 1D). Figure 1E presents an atomic force microscopy (AFM) image of a GMF with a lateral size of ~37 μm, which indicates that an as-synthesized GMF has an atomically smooth surface (RMS

https://doi.org/10.1021/acs.nanolett.2c00095
Nano Lett. 2022, 22, 1786−1794

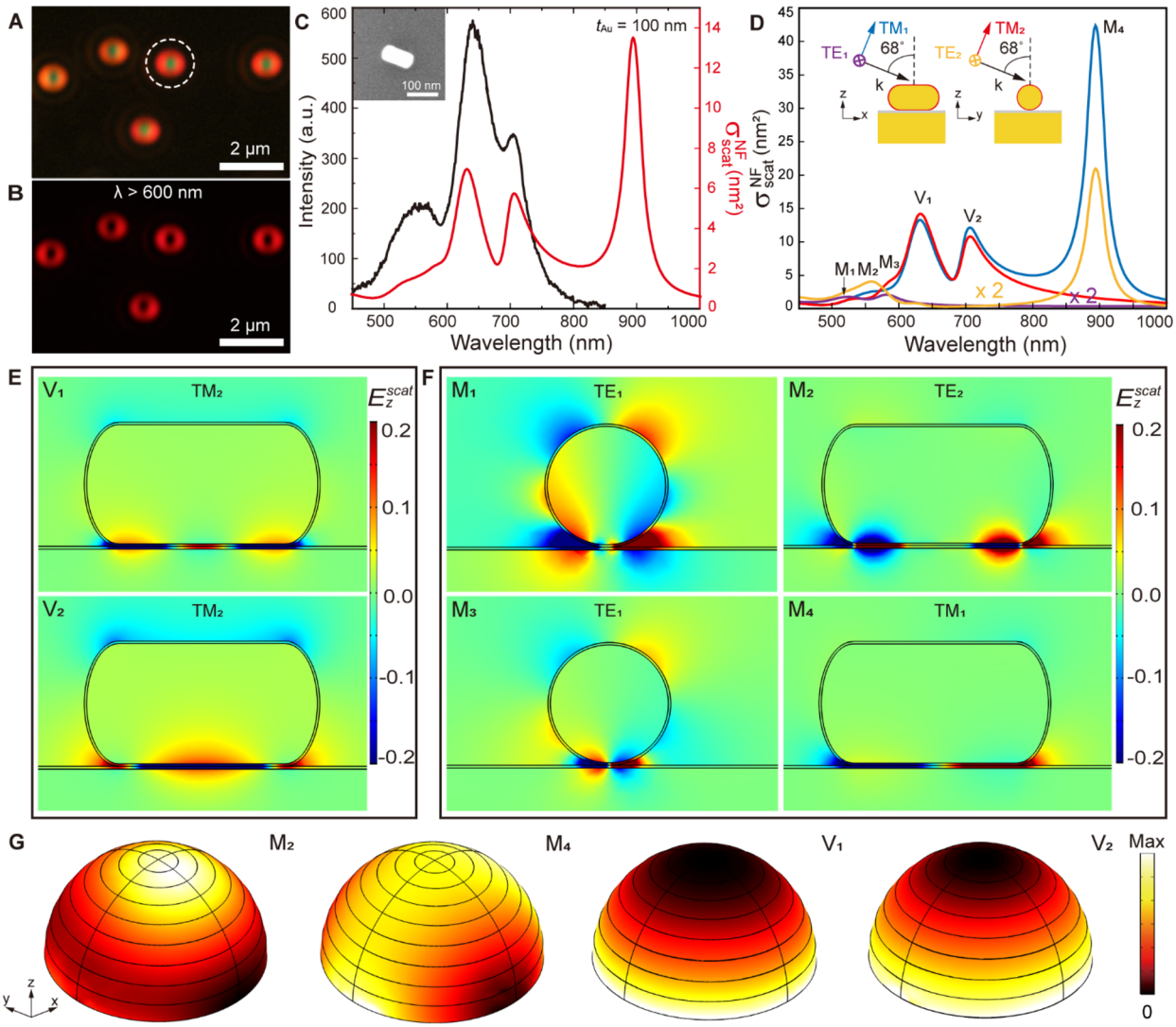

Figure 2. Cavity mode identification from scattering. (A, B) Dark-field scattering images of NRoMF nanocavities formed on a GMF with t_{Au} = 100 nm taken (A) without and (B) with a 600 nm long-pass filter. (C) Measured scattering spectrum (black line) of the nanocavity in (A) (circled) and calculated partial near-field scattering cross-section σ^{NF}_{scat} (red line) into a 50° collection angle, corresponding to the NA of the experimentally used objective. Inset: corresponding SEM image of the nanocavity. (D) Calculated σ^{NF}_{scat} of the NRoMF nanocavity under four different excitation conditions shown in the inset (note that the TE curves were magnified in 2 times). (E, F) Normalized E_z^{scat} distributions corresponding to the cavity modes labeled in (D). (G) Calculated energy angular scattering patterns of the nanocavity with the nanorod axis in the x direction, at the resonances corresponding to modes M_2, M_4, V_1, and V_2, respectively, at the same illumination conditions as in (E) and (F).

roughness ~0.2 nm) and a constant thickness (~23 nm) across the whole flake. A transmission electron microscopy (TEM) image of an edge of a GMF shows the existence of a native organic layer (~1 nm in thickness) on the surface of the GMFs (Figure 1F). Clear lattice fringes with the atomic planes spaced by 0.14 nm can be observed (Figure 1F, inset). Together with the electron diffraction pattern (Figure 1G), it confirms that the GMF is single crystalline and has a preferential growth direction along the [111] axis.[41] The excellent surface quality of GMFs together with the single crystallinity and tunable thickness makes GMFs extremely attractive for high-performance nanocavities.

GNRs, with average length and diameter of ~103 and 52 nm, were synthesized by a seed-mediated method (Supporting Information Section 2). Each GNR is capped with a bilayer of cetyltrimethylammonium bromide (CTAB) having a thickness of ~1 nm (Figure 1H). When deposited on a glass slide, individual GNRs appear as red spots in a dark-field scattering image (Figure 1I, inset), showing the longitudinal surface plasmon resonance peak blue-shifted to around 610 nm (cf., Figure 1I and Figure S2B). By drop-casting a diluted solution of GNRs onto GMFs on a glass slide, well-separated individual NRoMF nanocavities, with a total gap distance of ~2 nm, can be obtained (Figure 1J).

Cavity Mode Identification. Different from the scattering image of GNRs on a glass substrate, the nanocavities formed on a 100 nm thickness GMF (with the thickness much larger than the skin depth of gold) under the oblique illumination with an unpolarized white light (Figure 1A, see Supporting Information Section 3 for details) exhibit a distinct scattering image consisting of both green (in the middle) and red (with a doughnut-shaped spatial distribution) scattering components for each nanocavity (cf. inset of Figure 1I and Figure 2A,B). Correspondingly, the measured scattering spectrum (Figure 2C, black line) reveals three scattering peaks, locating at wavelengths of ~554, 641, and 706 nm, respectively.

https://doi.org/10.1021/acs.nanolett.2c00095
Nano Lett. 2022, 22, 1786−1794

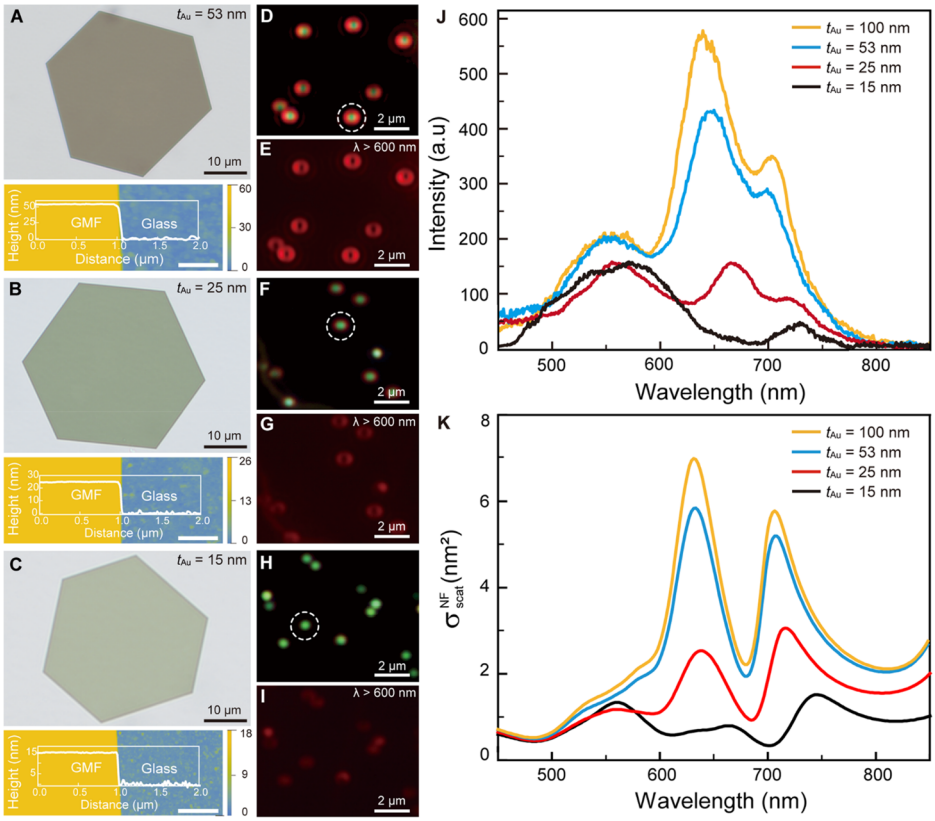

Figure 3. Effect of GMF thickness. (A–C) Optical micrographs of GMFs with t_{Au} of (A) 53, (B) 25, and (C) 15 nm, taken in transmission. Insets: corresponding AFM images and height profiles. Scale bar, 500 nm. (D–I) Dark-field scattering images of the NRoMF nanocavities formed on the GMFs in (A)–(C) taken (D, F, H) without and (E, G, I) with a 600 nm long-pass filter. (J) Scattering spectra of the single nanocavities (circled) shown in (D), (F), (H), and Figure 2A. (K) Calculated σ^{NF}_{scat} for the nanocavities with the GMF thickness of 100, 53, 25, and 15 nm.

To identify the observed modes, finite element numerical simulations of near-field scattering of the NRoMF nanocavities (Supporting Information Section 4) were performed for plane wave illumination at different nanorod orientations and light polarization configurations (inset of Figure 2D). This allows reconstruction of the experimental configuration with randomly oriented nanorods in the sample plane under unpolarized incident light by averaging the obtained plane wave scattering signals. Under TM_1 excitation (Figure 2D, blue line), there are four resonance peaks located at wavelengths of 560, 632, 706, and 895 nm, labeled as modes M_2, V_1, V_2, and M_4, respectively. However, in the case of TE_1 and TE_2 excitations (Figure 2D, violet and yellow lines), modes V_1 and V_2 are absent. This indicates that they correspond to vertically polarized resonances excited by the out-of-plane field component. The normalized z-components of the scattered electric field (E_z^{scat}) distributions of modes V_1 and V_2 (Figure 2E) show that the modes have three field maxima in the gap but with different field profiles. Mode V_1 has two dominant field maxima close to the edges of the rod, while for mode V_2, the dominant field maximum is in the middle. These modes are the results of the antibonding (high energy) and bonding (low energy) hybridizations, respectively, of the film-coupled vertical dipolar mode of the nanorod and the third-order (three antinodes) Fabry–Perot mode of a metal–insulator–metal (MIM) surface plasmon polariton (SPP) supported by the nanorod-film gap[42] (Supporting Information Section 5). As the wavelength of the MIM mode (approximately 60 nm for a vacuum wavelength of 650 nm) is much smaller than that in the free space , high-order MIM resonances are supported by the cavity even if it has a deep-subwavelength size. On the other hand, modes M_2 and M_4 can only be excited by TM_1 and TE_2 illuminations. The field distribution of mode M_4 (Figure 2F) shows that it has two field maxima with an opposite charge distribution in the gap, which is due to the coupling of the longitudinal nanorod mode with the antiphase image dipole induced in the GMF. Due to its symmetry and spectral position, it is hybridized with the second-order Fabry–Perot mode of the gap. For mode M_2, the E_z^{scat} distribution (Figure 2F) indicates that it is originated from the coupling of quadrupole mode of the nanorod with the sixth-order Fabry–Perot mode of the gap, which one can see more clearly from its E_x^{scat} distribution (Supporting Information Section 6). Under TE_1 and TM_2 excitations (Figure 2D), two relatively weak resonance peaks appear around 525 and 582 nm (M_1 and M_3). Taking into account their E_z^{scat} distributions (Figure 2F), one can further infer that these are film-coupled high-order transversal nanorod modes.[43] Thus, it is clear that the measured scattering peak around 554 nm is a mixture of M_1, M_2, and M_3 modes scattering predominantly in the top direction (Figure 2G), while the peaks around 641 and 706 nm are corresponding to the excitation of vertically oriented modes of V_1 and V_2 scattering predominantly in the side directions (Figure 2G).

In order to compare with the experimental result (Figure 2C, black line) measured under oblique illumination with an unpolarized white light (Figure 1A), a partial scattering spectrum of a nanocavity (Figure 2C, red line) was obtained

https://doi.org/10.1021/acs.nanolett.2c00095
Nano Lett. 2022, 22, 1786–1794

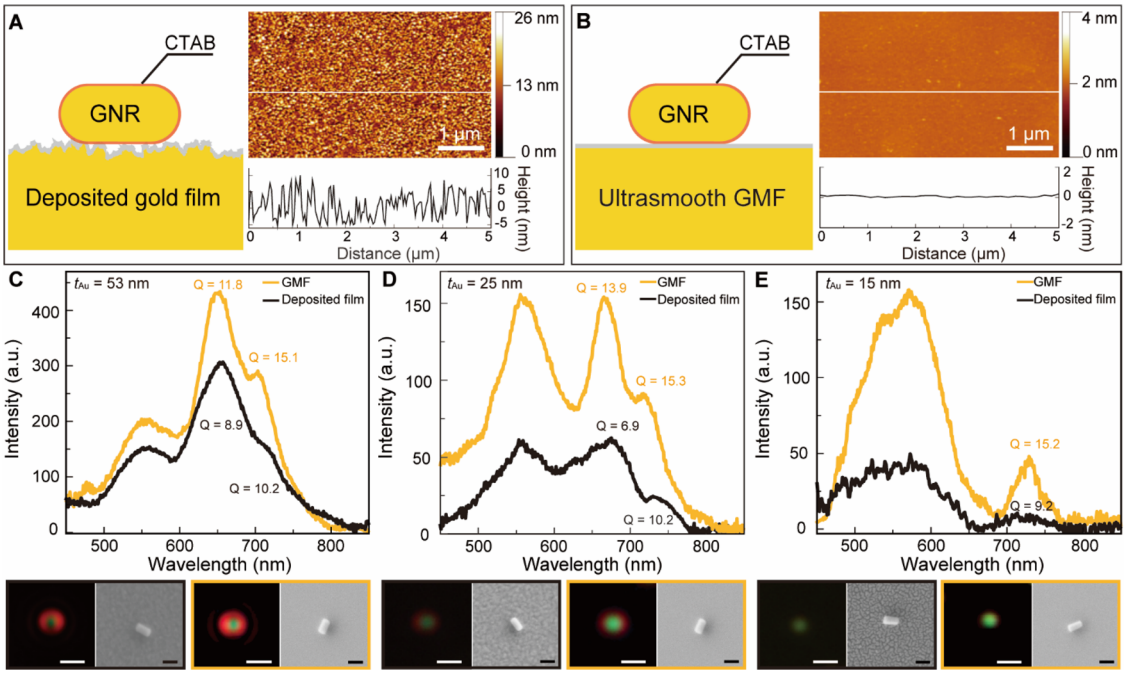

Figure 4. Effect of mirror quality. (A, B) Schematic illustrations of nanocavities formed on (A) a deposited gold film and (B) an ultrasmooth GMF. AFM images and line scans along the indicated white lines for a deposited gold film and a GMF with 15 nm thickness are also shown. (C−E) Comparison of the scattering spectra of the nanocavities formed on gold films and GMFs with t_{Au} of (C) 53 nm, (D) 25 nm, and (E) 15 nm. The quality factors of modes V_1 and V_2 are labeled correspondingly. Insets: the corresponding dark-field scattering and SEM images for the measured nanocavities on gold films (left panels) and GMFs (right panels), respectively. Scale bars in dark-field scattering images, 1 μm. Scale bars in SEM images, 100 nm.

by averaging the scattering spectra calculated under four different excitation conditions (Figure 2D). The calculated spectrum reproduces the experimental features well except the presence of an additional peak around 895 nm, which is due to the limited measurement capability of the setup at wavelengths larger than 850 nm. This peak is experimentally observed for structures with an increased gap thickness (Supporting Information Section 7).

Mirror-Thickness-Dependent Optical Response. Usually, NPoM nanocavities are constructed on metal films with thickness larger than the light penetration depth of the metal[12−19,21−23,25,26] (mainly due to the significantly deteriorated surface quality of optically thin metal films). The ability to fabricate high-quality optically thin (down to ∼10 nm) GMFs allows the investigation of the mirror-thickness-dependent optical response of the nanocavities. The thickness dependence should be important especially for the hybrid modes, affecting both coupling of the nanorod modes with the film and the MIM Fabry−Perot modes of the gap when the mirror thickness becomes smaller than the skin depth: for thicker films the MIM SPP modes are involved, while for thinner ones, insulator−metal−insulator (IMI) SPPs of the thin film become important. Figure 3A−C shows optical microscopy and AFM images of GMFs with thicknesses of 53, 25, and 15 nm, respectively. The transmittance of the GMFs increases gradually from 25% to 48% and 70% (around the wavelength of 510 nm, Supporting Information Section 8) with the decrease of GMF thickness. When the GMF thickness is 53 nm, the scattering image (Figure 3D,E) and spectrum (Figure 3J, blue line) of the NRoMF nanocavities are quite similar to those formed on GMFs with a 100 nm thickness (Figure 3J, yellow line) except a slight decrease in the intensity. However, with the further decrease of the GMF thickness down to 25 nm (Figure 3F,G) and 15 nm (Figure 3H,I), the doughnut-shaped scattering component fades out quickly while the inner green scattering component remains almost unchanged. Accordingly, the intensities of resonance peaks around 660 and 710 nm decrease quickly with the decrease of the GMF thickness (Figure 3J), while the intensity of the resonance peak around 560 nm remains almost constant.

The calculated evolution of near-field scattering spectra of NRoMF nanocavities with decreasing GMF thicknesses (Figure 3K) agree well with the experimental observation. With the decrease of the GMF thickness, the scattering intensities of modes V_1 and V_2 decrease first slowly (from 100 to 53 nm) and then dramatically down to ∼1/8 of the original values, while the intensity of the scattering peak around 560 nm stays almost at the same level. It can also be noted that as the GMF thickness gets smaller, the scattering intensity of mode M_4 decreases gradually (to ∼1/3 of the original value), along with a broadening in the line width (Figure S11 in Supporting Information). The significant modification of the far-field scattering properties of the nanocavities with the decrease of the thickness of optically thin GMFs can be understood as follows. Mode M_2 induces an antisymmetric charge distribution across the flake in the vicinity of the nanorod (see Figure S12 and Figure S13A), which with the opposite charges at the top and the bottom sides of the flake does not screen the fields of the quadrupolar component of the mode, so the latter effectively takes the form of a longitudinal dipolar mode of the nanorod radiating well both toward the collection objective and into the substrate with the decrease of the GMF thickness. At the same time, modes V_1, V_2, and M_4 induce a symmetric charge distribution across the flake (Figure S12) which on one hand keeps the nature of the mode the same and on the other hand couples well to the short-range

https://doi.org/10.1021/acs.nanolett.2c00095
Nano Lett. 2022, 22, 1786−1794

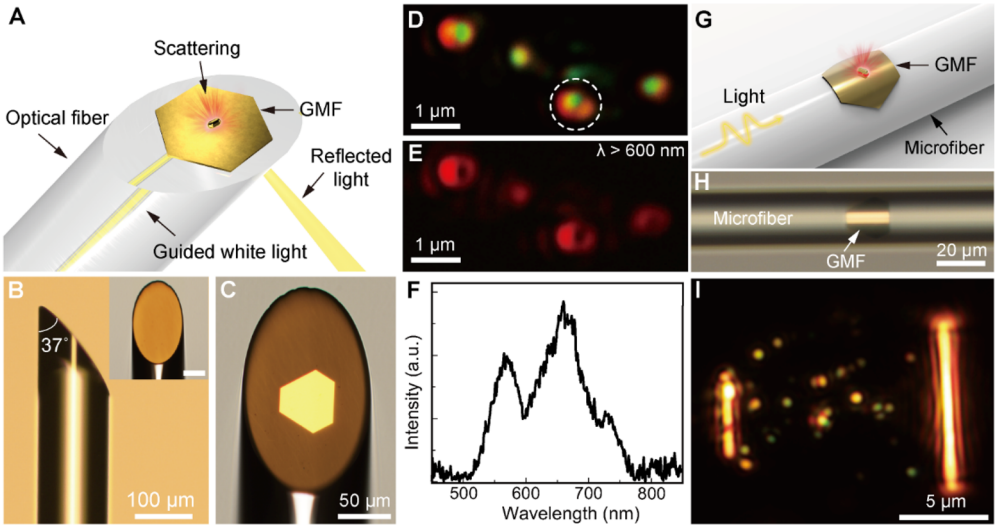

Figure 5. Integration with optical fibers. (A) Schematic diagram of the integration of NRoMF nanocavities with an angled fiber. (B, C) Optical micrographs of (B) a 37°-polished angled fiber (fabricated from a standard optical fiber, Corning SMF-28e), its polished surface (inset, the scale bar is 50 μm), and (C) the polished surface after transferring a GMF onto the fiber core. (D, E) Scattering images of fiber-excited NRoMF nanocavities taken (D) without and (E) with a 600 nm long-pass filter. (F) Scattering spectrum of a nanocavity (circled) in (D). (G) Schematic illustration of the integration of NRoMF nanocavities with a silica microfiber. (H) Optical micrograph of a GMF on a sidewall of a microfiber. (I) Scattering image of microfiber-integrated NRoMF nanocavities.

IMI SPP mode of the flake (Figure S13B–D for 15 nm thickness) as well as to the radiation into the substrate, thus resulting in the decrease of the radiation into the objective side. Therefore, this represents a new mechanism for engineering optical properties of NPoM nanocavities.

Effect of Mirror Quality. Due to the extreme confinement of optical fields in the nanometer-scale gap, NPoM nanocavities are very sensitive to the structural quality of the bottom metal mirrors.[36] We compared the performance of the nanocavities obtained with granular polycrystalline gold films (Figure 4A, left panel) and ultrasmooth single-crystalline GMFs (Figure 4B, left panel) with thicknesses of 15, 25, 53, and 100 nm, respectively. The superior surface quality of GMFs over the thermally deposited gold films (Supporting Information Section 10) can be clearly seen by comparing their SEM and AFM images. For small thicknesses the former are smooth and continuous, while the latter are rough and discontinuous (Figure S14). The measured RMS of the 15 nm thick GMF (~0.2 nm, Figure 4B) is much lower than that of the deposited gold films with thicknesses of 15, 25, 53, 100 nm (~4.1, 2.7, 1.4, and 1.1 nm, respectively, Figure 4A and Figure S15). As expected, there is a clear reduction in the line width of the scattering peaks (Figures 4C–E and Figure S17 for the mirror thickness of 100 nm), especially when the gold mirror is optically thin. More specifically, the quality factors (see Supporting Information Section 11 for calculation details) of modes V_1 and V_2 for the GMF-based nanocavities are about twice the values of the deposited film-based nanocavities when the mirror thicknesses are 25 and 15 nm (labeled in Figure 4D,E; see also the comparison in Table S1 in Supporting Information). At the same time, with the decrease of the film thickness from 100 nm to 53, 25, and 15 nm, the ratio of the scattering intensities between the two cases (GMF vs deposited film) increases from ~1.2 to 1.3, 2.8, and 3.2, respectively. The great improvement in the optical qualities of NRoMF nanocavities by the use of ultrasmooth single-crystalline GMFs (especially when they are optically thin) can be attributed to the reduction in electron scattering losses introduced by surface roughness and grain boundaries[30,31,33−35] which are significant in granular polycrystalline deposited gold films. In addition, compared with nanocavities formed on a rough deposited film, nanocavities formed on GMFs have a much more uniform dielectric gap thickness across the whole cavity, which is also beneficial for achieving optical modes closer to the designed characteristics and for the decrease of an inhomogeneous broadening line width in a nanoparticle ensemble. Thus, optically thin GMFs with single-crystalline structure and excellent surface smoothness provide an ideal platform for the realization of low-loss nanocavities that approach the theoretical optical quality limit, determined by the inevitable ohmic loss and radiative damping of the modes (Table S1 in Supporting Information for the comparison of quality factors of modes V_1 and V_2 derived from the experimental and calculated results).

Integration with Optical Fibers. To date, due to the use of nontransparent thick metallic mirrors (limited by the ability to fabricate high-quality optically thin metal films), NPoM nanocavities are commonly excited from the nanoparticle side with bulky optical microscopy systems,[4] making it difficult to realize miniaturized and integrated nanocavity-based photonic devices for practical applications. At the same time, as shown in Figure S12, optically thin and double-sided ultrasmooth GMFs provide an opportunity for the excitation and out-coupling of nanocavity modes from the mirror side with high efficiency and low loss due to the enhanced penetration of nanocavity modes into the substrate. Taking advantage of the transferable property of the chemically synthesized GMFs, low-loss NRoMF nanocavities could be readily integrated with other optical systems such as the mature platform of fiber optics. Figure 5A shows a schematic illustration of the integration of nanocavities with a cleaved optical fiber, in which nanocavities can be compactly excited by the guided light from the microflake side. Experimentally, we used a 37° polished angled fiber (Figure 5B) with a good surface quality (inset). It gives the advantage of the background-free excitation of plasmonic nanocavities by the evanescent fields of the totally

https://doi.org/10.1021/acs.nanolett.2c00095
Nano Lett. 2022, 22, 1786−1794

internally reflected guided light at the interface[44,45] (it is worth noting, though, that nanocavities can also be excited through the substrate with the transmitted light without the use of a total internal reflection configuration). To construct nanocavities on the surface, a GMF with a thickness of 40 nm was first transferred onto the fiber core (Figure 5C and Supporting Information Section 12), followed by drop-casting of a diluted GNR solution to obtain sparsely dispersed nanocavities. Upon the launching of an unpolarized white light into the optical fiber, clear scattering spots were observed from the surface of the GMF (Figure 5D,E), which have the similar scattering pattern and spectrum (Figure 5F) with nanocavities excited by a dark-field spectroscopy (Figure 3). Nanocavities can also be integrated with a microscale waveguide, e.g., a silica microfiber (Figure 5G). Figure 5H presents an optical micrograph of a silica microfiber (20 μm in diameter) covered with a GMF (~20 nm in thickness) conformally on the sidewall (see Supporting Information Section 13 for details). Sparsely dispersed nanocavities can be efficiently excited by a waveguided unpolarized white light in the microfiber, as indicated by the scattering spots on the GMF (Figure 5I). Although fiber-integrated nanocavities can also be realized by the use of deposited gold films, the approach demonstrated here provides straightforward advantages including superior optical quality, easy fabrication, and low cost.

CONCLUSIONS

We have shown that single-crystalline GMFs with atomically smooth surface and tunable thickness offer an ideal platform for integratable low-loss NPoM nanocavities. The superior optical quality and mode tunability of nanocavities afforded by the atomically smooth single-crystalline GMFs can open new opportunities for pushing the limits of plasmonic nanocavity-based techniques and inspiring plasmonic devices with superior performance. Also, the ability to integrate the extreme nanophotonic platform of NPoM nanocavities with the mature platform of fiber optics or micro/nanowaveguides, with excitation through the optically thin ultrasmooth mirror, makes it possible to develop miniaturized nanocavity-based photonic devices, such as sensors, modulators, and light sources, with high performance and low cost.

ASSOCIATED CONTENT

Supporting Information

The Supporting Information is available free of charge at https://pubs.acs.org/doi/10.1021/acs.nanolett.2c00095.

Synthesis of GMFs and GNRs; dark-field spectroscopy setup; numerical simulations; formation of modes V_1 and V_2; E_x^{scat} field distribution of mode M_2; effect of spacer thickness on the optical properties; transmittance of GMFs with different thicknesses; scattering cross-sections and field distributions of nanocavities on GMFs with various thicknesses; deposition and characterization of gold films; comparison of quality factors; transfer of GMFs onto an angled fiber; integration with an optical microfiber (PDF)

AUTHOR INFORMATION

Corresponding Authors

Pan Wang − *State Key Laboratory of Modern Optical Instrumentation, College of Optical Science and Engineering, Zhejiang University, Hangzhou 310027, China;* orcid.org/0000-0003-4209-5186; Email: nanopan@zju.edu.cn

Anatoly V. Zayats − *Department of Physics and London Centre for Nanotechnology, King's College London, London WC2R 2LS, U.K.;* orcid.org/0000-0003-0566-4087; Email: a.zayats@kcl.ac.uk

Limin Tong − *State Key Laboratory of Modern Optical Instrumentation, College of Optical Science and Engineering, Zhejiang University, Hangzhou 310027, China;* Email: phytong@zju.edu.cn

Authors

Lufang Liu − *State Key Laboratory of Modern Optical Instrumentation, College of Optical Science and Engineering, Zhejiang University, Hangzhou 310027, China*

Alexey V. Krasavin − *Department of Physics and London Centre for Nanotechnology, King's College London, London WC2R 2LS, U.K.;* orcid.org/0000-0003-2522-5735

Junsheng Zheng − *State Key Laboratory of Modern Optical Instrumentation, College of Optical Science and Engineering, Zhejiang University, Hangzhou 310027, China*

Yuanbiao Tong − *State Key Laboratory of Modern Optical Instrumentation, College of Optical Science and Engineering, Zhejiang University, Hangzhou 310027, China*

Xiaofei Wu − *NanoOptics & Biophotonics Group, Experimentelle Physik 5, Physikalisches Institut, Universität Würzburg, 97074 Würzburg, Germany;* orcid.org/0000-0002-4594-1678

Bert Hecht − *NanoOptics & Biophotonics Group, Experimentelle Physik 5, Physikalisches Institut, Universität Würzburg, 97074 Würzburg, Germany*

Chenxinyu Pan − *State Key Laboratory of Modern Optical Instrumentation, College of Optical Science and Engineering, Zhejiang University, Hangzhou 310027, China*

Jialin Li − *State Key Laboratory of Modern Optical Instrumentation, College of Optical Science and Engineering, Zhejiang University, Hangzhou 310027, China*

Linjun Li − *State Key Laboratory of Modern Optical Instrumentation, College of Optical Science and Engineering, Zhejiang University, Hangzhou 310027, China;* orcid.org/0000-0002-2734-0414

Xin Guo − *State Key Laboratory of Modern Optical Instrumentation, College of Optical Science and Engineering, Zhejiang University, Hangzhou 310027, China*

Complete contact information is available at: https://pubs.acs.org/10.1021/acs.nanolett.2c00095

Author Contributions

[‖]L.L. and A.V.K. contributed equally to this work. P.W. and L.T. conceived the study and co-supervised the project with A.V.Z. L.L. constructed the experiment and performed the measurements. C.P. synthesized gold microflakes under supervision of X.W. and B.H., and Y.T. transferred gold microflakes onto optical fibers. J.L. deposited the gold films. A.V.K. and J.Z. performed numerical simulations. P.W., A.V.K., A.V.Z., and L.T. analyzed the data. All the authors discussed the results and co-wrote the paper. All authors have given approval to the final version of the manuscript.

Funding

This research was supported by the National Natural Science Foundation of China (Grants 62075195 and 12004333), National Key Research and Development Project of China (Grant 2018YFB2200404), ERC iCOMM Project (Grant

789340), and Fundamental Research Funds for the Central Universities.

Notes

The authors declare no competing financial interest.

REFERENCES

(1) Gramotnev, D. K.; Bozhevolnyi, S. I. Plasmonics beyond the diffraction limit. *Nat. Photonics* **2010**, *4* (2), 83−91.
(2) Schuller, J. A.; Barnard, E. S.; Cai, W.; Jun, Y. C.; White, J. S.; Brongersma, M. L. Plasmonics for extreme light concentration and manipulation. *Nat. Mater.* **2010**, *9* (3), 193−204.
(3) Yang, Y.; Gu, C.; Li, J. Sub-5 nm metal nanogaps: physical properties, fabrication methods, and device applications. *Small* **2019**, *15* (5), 1804177.
(4) Li, G.; Zhang, Q.; Maier, S. A.; Lei, D. Plasmonic particle-on-film nanocavities: a versatile platform for plasmon-enhanced spectroscopy and photochemistry. *Nanophotonics* **2018**, *7* (12), 1865−1889.
(5) Baumberg, J. J.; Aizpurua, J.; Mikkelsen, M. H.; Smith, D. R. Extreme nanophotonics from ultrathin metallic gaps. *Nat. Mater.* **2019**, *18* (7), 668−678.
(6) Ciracì, C.; Hill, R. T.; Mock, J. J.; Urzhumov, Y.; Fernández-Domínguez, A. I.; Maier, S. A.; Pendry, J. B.; Chilkoti, A.; Smith, D. R. Probing the ultimate limits of plasmonic enhancement. *Science* **2012**, *337* (6098), 1072.
(7) Tserkezis, C.; Esteban, R.; Sigle, D. O.; Mertens, J.; Herrmann, L. O.; Baumberg, J. J.; Aizpurua, J. Hybridization of plasmonic antenna and cavity modes: extreme optics of nanoparticle-on-mirror nanogaps. *Phys. Rev. A* **2015**, *92* (5), 053811.
(8) Benz, F.; Schmidt, M. K.; Dreismann, A.; Chikkaraddy, R.; Zhang, Y.; Demetriadou, A.; Carnegie, C.; Ohadi, H.; de Nijs, B.; Esteban, R.; Aizpurua, J.; Baumberg, J. J. Single-molecule optomechanics in "picocavities". *Science* **2016**, *354* (6313), 726−729.
(9) Chen, W.; Zhang, S.; Kang, M.; Liu, W.; Ou, Z.; Li, Y.; Zhang, Y.; Guan, Z.; Xu, H. Probing the limits of plasmonic enhancement using a two-dimensional atomic crystal probe. *Light Sci. Appl.* **2018**, *7* (1), 56.
(10) Nordlander, P.; Prodan, E. Plasmon Hybridization in Nanoparticles near Metallic Surfaces. *Nano Lett.* **2004**, *4* (11), 2209−2213.
(11) Hill, R. T.; Mock, J. J.; Hucknall, A.; Wolter, S. D.; Jokerst, N. M.; Smith, D. R.; Chilkoti, A. Plasmon ruler with angstrom length resolution. *ACS Nano* **2012**, *6* (10), 9237−9246.
(12) Moreau, A.; Ciracì, C.; Mock, J. J.; Hill, R. T.; Wang, Q.; Wiley, B. J.; Chilkoti, A.; Smith, D. R. Controlled-reflectance surfaces with film-coupled colloidal nanoantennas. *Nature* **2012**, *492* (7427), 86−89.
(13) Russell, K. J.; Liu, T.-L.; Cui, S.; Hu, E. L. Large spontaneous emission enhancement in plasmonic nanocavities. *Nat. Photonics* **2012**, *6* (7), 459−462.
(14) Rodríguez-Fortuño, F. J.; Marino, G.; Ginzburg, P.; O'Connor, D.; Martínez, A.; Wurtz, G. A.; Zayats, A. V. Near-field interference for the unidirectional excitation of electromagnetic guided modes. *Science* **2013**, *340* (6130), 328−330.
(15) Akselrod, G. M.; Argyropoulos, C.; Hoang, T. B.; Ciracì, C.; Fang, C.; Huang, J.; Smith, D. R.; Mikkelsen, M. H. Probing the mechanisms of large Purcell enhancement in plasmonic nanoantennas. *Nat. Photonics* **2014**, *8* (11), 835−840.
(16) Chikkaraddy, R.; de Nijs, B.; Benz, F.; Barrow, S. J.; Scherman, O. A.; Rosta, E.; Demetriadou, A.; Fox, P.; Hess, O.; Baumberg, J. J. Single-molecule strong coupling at room temperature in plasmonic nanocavities. *Nature* **2016**, *535* (7610), 127−130.
(17) Hoang, T. B.; Akselrod, G. M.; Mikkelsen, M. H. Ultrafast room-temperature single photon emission from quantum dots coupled to plasmonic nanocavities. *Nano Lett.* **2016**, *16* (1), 270−275.
(18) Chen, X.; Chen, Y.; Qin, J.; Zhao, D.; Ding, B.; Blaikie, R. J.; Qiu, M. Mode modification of plasmonic gap resonances induced by strong coupling with molecular excitons. *Nano Lett.* **2017**, *17* (5), 3246−3251.
(19) Chen, W.; Zhang, S.; Deng, Q.; Xu, H. Probing of sub-picometer vertical differential resolutions using cavity plasmons. *Nat. Commun.* **2018**, *9* (1), 801.
(20) Wang, P.; Krasavin, A. V.; Nasir, M. E.; Dickson, W.; Zayats, A. V. Reactive tunnel junctions in electrically driven plasmonic nanorod metamaterials. *Nat. Nanotechnol.* **2018**, *13* (2), 159−164.
(21) Parzefall, M.; Szabó, Á.; Taniguchi, T.; Watanabe, K.; Luisier, M.; Novotny, L. Light from Van der Waals quantum tunneling devices. *Nat. Commun.* **2019**, *10* (1), 292.
(22) Peng, J.; Jeong, H.-H.; Lin, Q.; Cormier, S.; Liang, H.-L.; De Volder, M. F.; Vignolini, S.; Baumberg, J. J. Scalable electrochromic nanopixels using plasmonics. *Sci. Adv.* **2019**, *5* (5), No. eaaw2205.
(23) Yang, Y.; Zhu, D.; Yan, W.; Agarwal, A.; Zheng, M.; Joannopoulos, J. D.; Lalanne, P.; Christensen, T.; Berggren, K. K.; Soljačić, M. A general theoretical and experimental framework for nanoscale electromagnetism. *Nature* **2019**, *576* (7786), 248−252.
(24) Li, C.; Duan, S.; Wen, B.; Li, S.; Kathiresan, M.; Xie, L.; Chen, S.; Anema, J. R.; Mao, B.; Luo, Y.; Tian, Z.; Li, J. Observation of inhomogeneous plasmonic field distribution in a nanocavity. *Nat. Nanotechnol.* **2020**, *15* (11), 922−926.
(25) Qin, J.; Chen, Y.; Zhang, Z.; Zhang, Y.; Blaikie, R. J.; Ding, B.; Qiu, M. Revealing strong plasmon-exciton coupling between nanogap resonators and two-dimensional semiconductors at ambient conditions. *Phys. Rev. Lett.* **2020**, *124* (6), 063902.
(26) Li, G.; Lei, D.; Qiu, M.; Jin, W.; Lan, S.; Zayats, A. V. Light-induced symmetry breaking for enhancing second-harmonic generation from an ultrathin plasmonic nanocavity. *Nat. Commun.* **2021**, *12* (1), 4326.
(27) Xiong, Y.; Fu, T.; Zhang, D.; Zhang, S.; Xu, H. Superradiative plasmonic nanoantenna biosensors enable sensitive immunoassay using the naked eye. *Nanoscale* **2021**, *13* (4), 2429−2435.
(28) Huang, J.; Grys, D.-B.; Griffiths, J.; de Nijs, B.; Kamp, M.; Lin, Q.; Baumberg, J. J. Tracking interfacial single-molecule pH and binding dynamics via vibrational spectroscopy. *Sci. Adv.* **2021**, *7* (23), No. eabg1790.
(29) Wright, D.; Lin, Q.; Berta, D.; Földes, T.; Wagner, A.; Griffiths, J.; Readman, C.; Rosta, E.; Reisner, E.; Baumberg, J. J. Mechanistic study of an immobilized molecular electrocatalyst by in situ gap-plasmon-assisted spectro-electrochemistry. *Nat. Catal.* **2021**, *4* (2), 157−163.
(30) Ditlbacher, H.; Hohenau, A.; Wagner, D.; Kreibig, U.; Rogers, M.; Hofer, F.; Aussenegg, F. R.; Krenn, J. R. Silver nanowires as surface plasmon resonators. *Phys. Rev. Lett.* **2005**, *95* (25), 257403.
(31) Nagpal, P.; Lindquist, N. C.; Oh, S.-H.; Norris, D. J. Ultrasmooth patterned metals for plasmonics and metamaterials. *Science* **2009**, *325* (5940), 594−597.
(32) Chen, K.-P.; Drachev, V. P.; Borneman, J. D.; Kildishev, A. V.; Shalaev, V. M. Drude relaxation rate in grained gold nanoantennas. *Nano Lett.* **2010**, *10* (3), 916−922.
(33) Lin, L.; Chen, M.; Qin, H.; Peng, X. Ag nanocrystals with nearly ideal optical quality: synthesis, growth mechanism, and characterizations. *J. Am. Chem. Soc.* **2018**, *140* (50), 17734−17742.
(34) Maniyara, R. A.; Rodrigo, D.; Yu, R.; Canet-Ferrer, J.; Ghosh, D. S.; Yongsunthon, R.; Baker, D. E.; Rezikyan, A.; García de Abajo, F. J.; Pruneri, V. Tunable plasmons in ultrathin metal films. *Nat. Photonics* **2019**, *13* (5), 328−333.
(35) Abd El-Fattah, Z. M.; Mkhitaryan, V.; Brede, J.; Fernández, L.; Li, C.; Guo, Q.; Ghosh, A.; Echarri, A. R.; Naveh, D.; Xia, F.; Ortega, J. E.; García de Abajo, F. J. Plasmonics in Atomically Thin Crystalline Silver Films. *ACS Nano* **2019**, *13* (7), 7771−7779.
(36) Lumdee, C.; Yun, B.; Kik, P. G. Effect of surface roughness on substrate-tuned gold nanoparticle gap plasmon resonances. *Nanoscale* **2015**, *7* (9), 4250−4255.
(37) Hegner, M.; Wagner, P.; Semenza, G. Ultralarge atomically flat template-stripped Au surfaces for scanning probe microscopy. *Surf. Sci.* **1993**, *291* (1−2), 39−46.

https://doi.org/10.1021/acs.nanolett.2c00095
Nano Lett. 2022, 22, 1786−1794

(38) Vogel, N.; Zieleniecki, J.; Köper, I. As flat as it gets: ultrasmooth surfaces from template-stripping procedures. *Nanoscale* **2012**, *4* (13), 3820−3832.
(39) Kern, J.; Großmann, S.; Tarakina, N. V.; Häckel, T.; Emmerling, M.; Kamp, M.; Huang, J.-S.; Biagioni, P.; Prangsma, J. C.; Hecht, B. Atomic-scale confinement of resonant optical fields. *Nano Lett.* **2012**, *12* (11), 5504−5509.
(40) Huang, J.-S.; Callegari, V.; Geisler, P.; Brüning, C.; Kern, J.; Prangsma, J. C.; Wu, X.; Feichtner, T.; Ziegler, J.; Weinmann, P.; Kamp, M.; Forchel, A.; Biagioni, P.; Sennhauser, U.; Hecht, B. Atomically flat single-crystalline gold nanostructures for plasmonic nanocircuitry. *Nat. Commun.* **2010**, *1* (1), 150.
(41) Krauss, E.; Kullock, R.; Wu, X.; Geisler, P.; Lundt, N.; Kamp, M.; Hecht, B. Controlled growth of high-aspect-ratio single-crystalline gold platelets. *Cryst. Growth Des.* **2018**, *18* (3), 1297−1302.
(42) Sugimoto, H.; Yashima, S.; Fujii, M. Hybridized plasmonic gap mode of gold nanorod on mirror nanoantenna for spectrally tailored fluorescence enhancement. *ACS Photonics* **2018**, *5* (8), 3421−3427.
(43) Li, G.; Zhang, Y.; Lei, D. Hybrid plasmonic gap modes in metal film-coupled dimers and their physical origins revealed by polarization resolved dark field spectroscopy. *Nanoscale* **2016**, *8* (13), 7119−7126.
(44) Mock, J. J.; Hill, R. T.; Degiron, A.; Zauscher, S.; Chilkoti, A.; Smith, D. R. Distance-dependent plasmon resonant coupling between a gold nanoparticle and gold film. *Nano Lett.* **2008**, *8* (8), 2245−2252.
(45) Mock, J. J.; Hill, R. T.; Tsai, Y.-J.; Chilkoti, A.; Smith, D. R. Probing dynamically tunable localized surface plasmon resonances of film-coupled nanoparticles by evanescent wave excitation. *Nano Lett.* **2012**, *12* (4), 1757−1764.

https://doi.org/10.1021/acs.nanolett.2c00095
Nano Lett. 2022, 22, 1786−1794